

# A Search for X-Ray Flashes with *XMM-Newton*

Nicholas M. Law<sup>1,2</sup>, Robert E. Rutledge<sup>2</sup> and Shrinivas R. Kulkarni<sup>2</sup>,

## ABSTRACT

We searched for X-ray flashes (XRFs) – which we defined as  $\sim 10$  s duration transient X-ray events observable in the 0.4-15 keV passband – in fields observed using *XMM-Newton* with the EPIC/pn detector. While we find two non-Poissonian events, the astrophysical nature of the events is not confirmed in fully simultaneous observations with the EPIC/MOS detectors, and we conclude that the events are anomalous to the EPIC/pn detector. We find a 90% upper limit on the number of flashes per sky per year at two different incoming flash fluxes:  $6.2 \times 10^9$  events sky<sup>-1</sup> yr<sup>-1</sup> for a flux of  $7.1 \times 10^{-13}$  erg cm<sup>-2</sup> s<sup>-1</sup> and  $1.0 \times 10^8$  events sky<sup>-1</sup> yr<sup>-1</sup> for  $1.4 \times 10^{-11}$  erg cm<sup>-2</sup> s<sup>-1</sup> both assuming a spectral power-law photon index  $\alpha=2$ . These limits are consistent with an extrapolation from the *BeppoSAX*/WFC XRF rate at much higher fluxes ( $\sim$  a factor of  $10^5$ ), assuming an homogenous population, and with a previous, more stringent limit derived from ROSAT pointed observations.

## 1. Introduction

Observations of large areas of the sky in the X-ray (1-20 keV) and gamma-ray (20-1000 keV) passbands have found bursts of X-rays – X-ray flashes (XRFs) – which are observationally distinct, but may be related to, the ubiquitous and relatively well-studied gamma-ray bursts (GRBs). The phenomenological definition of these events, proposed by Heise et al. (2002) (H02 hereafter), includes strong 2-10 keV emission, in which the 2-10 keV fluence is greater than the 50-300 keV fluence; a duration of  $\lesssim$  few  $10^3$  s (to distinguish from flare-stars); and the absence of a strong optical or IR counterpart (to distinguish from X-ray binaries and coronally active stars). These phenomena have recently been surveyed H02 using *BeppoSAX*/WFC observations (2-25 keV sensitivity) over 6 years and a  $40 \times 40$  sq deg field of view. This resulted in a detection of 34 of these events, with typical X-ray fluxes of  $10^{-8}$  erg cm<sup>-2</sup> s<sup>-1</sup> (2-20 keV).

---

<sup>1</sup>Institute of Astronomy, Madingley Road, Cambridge CB3 0HA, UK; nml27@ast.cam.ac.uk

<sup>2</sup>Division of Physics, Mathematics and Astronomy, California Institute of Technology, MS 130-33, Pasadena, CA 91125; rutledge@tapir.caltech.edu, srk@astro.caltech.edu

XRFs can be observationally distinguished from the well-studied type-I X-ray bursts, which are due to thermonuclear flashes on the surfaces of neutron stars (NSs) in accreting low-mass X-ray binaries (see Lewin et al. 1993 for a review); the type-I X-ray bursts have  $\approx 1$  s rise-times and exponential decays with characteristic timescales of 10-100 s, during which the thermal spectrum softens as the NS atmosphere cools. XRFs, by contrast, have non-thermal spectra, and their lightcurves typically do not follow a fast-rise/exponential decay time profile.

At present, the origin of the XRFs is unclear. Some GRB models permit similar bursts at lower photon energies, by altering just one parameter of the model. An example of such a model is the so-called hypernova model, in which the details of the characteristics of the progenitor star (e.g. mass, spin) may play a critical role in determining the energy band of the prompt emission. In such a case, the XRFs would originate from a similar parent population to the GRBs (at cosmological distances, in star-forming galaxies), and thus share some observational properties with GRBs – such as an homogenous distribution on the sky, and a break in the logN–logS cumulative distribution due to cosmological (and, perhaps, source population) evolution. Another example of a GRB-origin model which can produce the XRFs is to place the GRBs at high redshift, so that the spectral energy distribution peaks at a lower energy. However, the optical detection of the host galaxies associated with XRF 011030 (Fruchter et al. 2002a) and XRF 020427 (Fruchter et al. 2002b) make this explanation less likely. Other GRB models – such as inspiralling binary NSs, which may not vary in the energy band where most of their energy is emitted – may not be able to accommodate the XRF phenomena, in which case the XRFs could originate from a distinct population.

Data accumulated from X-ray satellites may contain previously unrecognized X-ray flashes (unresolved transients lasting  $O[10\text{--}100\text{ s}]$ ). Events with characteristics similar to X-ray flashes have been claimed detected in *Einstein* observatory data (Gotthelf et al. 1996), down to  $10^{-11}\text{ erg cm}^{-2}\text{ s}^{-1}$  in  $1.5\times 10^7\text{ s}$  of data (0.2–3.5 keV) for a  $1\text{ deg}^2$  FOV, for a total integration of  $1.5\times 10^7\text{ s deg}^2$ , in which 42 events were detected; the implied burst rate is  $3.7\times 10^6\text{ events sky}^{-1}\text{ yr}^{-1}$  at a fluence of  $2\times 10^{-10}\text{ erg cm}^{-2}\text{ event}^{-1}$ . A search with *ROSAT*/PSPC (Vikhlinin 1998) with a comparable exposure and flux limit ( $1.6\times 10^7\text{ s}$ ,  $2.7\text{ deg}^2$  FOV, 0.1–2.4 keV) found no bursts, producing a 90% confidence upper-limit ( $<2$  bursts) of  $6.1\times 10^4\text{ events sky}^{-1}\text{ yr}^{-1}$  above a fluence of  $2.6\times 10^{-10}\text{ erg cm}^{-2}\text{ event}^{-1}$ , which contradicts the *Einstein* result.

The new generation of sensitive X-ray observatories (*Chandra*, *XMM-Newton*) offer a new opportunity to search for these events. We performed such a search using *XMM-Newton*-EPIC/pn; although we find two non-Poissonian events, their astrophysical

origin is not confirmed with fully simultaneous observation with *XMM*-Newton-EPIC/MOS; we conclude that the events are anomalous to the EPIC/pn detector. We subsequently set upper-limits for the full-sky XRF rate.

The paper is organized as follows. In § 2, we estimate detectable burst rates for sensitive X-ray observatories, finding that the most sensitive instrument to the phenomenon is the *XMM*-Newton EPIC/pn detector. In § 3, we describe the *XMM*-Newton dataset we used, and the detection algorithm, together with source characterization procedures and XRF detection sensitivity calculations. In § 4 we give the results of our search, and describe the XRF detection sensitivity. We discuss these results in § 5 and conclude in § 6.

## 2. Observational Burst Rate Estimates

The feasibility of detection of XRFs with a particular instrument may be extrapolated from the number of flashes detected with SAX/WFC (H02). Assuming the objects producing the flashes are isotropically and homogeneously distributed the number of detectable flashes scales as

$$\frac{N(> F_1)}{N(> F_2)} = \left(\frac{F_1}{F_2}\right)^{-\frac{3}{2}} \quad (1)$$

where  $F_1$  and  $F_2$  are the flux limits of the detectors and  $N(> F_1)$  and  $N(> F_2)$  are the numbers of flashes detected at those flux limits.

We assume a significant detection requires a minimum flux corresponding to one count per second at the detector chip. This flux was found from WebPIMMS<sup>3</sup> and is dependent on the spectral shape of the flash, which we took to be a photon spectral slope between  $\alpha=1.2$ – $2.0$ , as observed with SAX/WFC (Heise & in 't Zand 2001). Data from the Chandra ACIS and the *XMM*-Newton EPIC/pn and MOS cameras are available to us in public archives. Using Eqn. 1 the total XRFs per sky per year at a given flux rate (and so a given detector sensitivity) were extrapolated from those observed with SAX/WFC. Using the power-law photon index range observed with SAX/WFC, the solid angle field-of-view of the detectors, and the total integrated time using each detector, we calculated expected detectable number of events (Table 1) in the presently available data.

---

<sup>3</sup><http://heasarc.gsfc.nasa.gov/Tools/w3pimms.html>

The XMM-Newton EPIC/pn detector offers the greatest chance of flash detection in available data. We focus on the EPIC/pn detector, but it should be noted that our algorithms are applicable to other datasets and can be used, for example, without modification with EPIC MOS data. Depending on the spectrum, the EPIC/MOS1+2 detectors (together) have  $\sim 50\%$  of the effective area of the EPIC/pn detector. As the MOS and pn detectors observe the same region of sky simultaneously, coincidence of events on both detectors will be used for confirmation of the astrophysical origin of transients.

### 3. XMM-Newton Data and Analysis

#### 3.1. Data set

Observations were selected from the *XMM*-Newton Science Data Archive<sup>4</sup> based on the following criteria:

1. We use observations publicly or otherwise available to us on 2002 June 1;
2. Observations with  $> 50$  ks total observation time. Extension to smaller observation times increases the chance of flash detection proportional to the total integration time, but at an increased overhead of file handling and data collation; 50 ks was chosen as a compromise value.
3. Observations within  $15^\circ$  latitude to the Galactic equator were excluded to reduce the incidence of transients from Galactic sources (X-ray binaries, for example).

From these, we analysed 225.1 ks of observations, split into 6 separate observations with total livetimes ranging from 19939 s to 47721 s.

Simulations using WebPIMMS and the observed background spectrum suggested that detection sensitivity would be increased by removing counts with energies below 0.4 keV. We therefore only consider counts between 0.4 and 15 keV.

#### 3.2. XRF Detection

An outline of our XRF detection algorithm is as follows. We split observation event lists into short sections of time, with duration of 500 s, with 100 s of overlap between adjacent

---

<sup>4</sup>*XMM*-Newton Science Operations Center, <http://xmm.vilspa.esa.es>

sections. Within each time section, we bin counts into a  $256 \times 256 \times 256$  bin data cube. Each bin volume is  $9.95'' \times 9.95''$  spatially and has a duration of 2.34 s. We thus oversample both the point-spread-function (PSF;  $\sim 50''$ ) and the desired optimal burst duration. We took this duration to be 10 s, which importantly affects the duration of transients to which this search is sensitive.

A 3-dimensional sliding *celldetect* algorithm is used to search for volumes (corresponding to 1 PSF spatially and one transient duration temporally) which have a significantly elevated count rate compared to their local background. The local background is estimated from the count in the adjacent  $3 \text{ PSF} \times 3 \text{ transient duration}$  volume surrounding the test volume (that is, a spatio-temporal integration which is  $26\times$  as large as the test volume). Poisson statistics are used to determine the significance of the local counts given the background. Bins in which the fractional value of the detector exposure map is  $< 0.35$  (where 1.0 is an exposure time equal to the total detector exposure time) are ignored.

The algorithm calculates the local count significances throughout the binned cube, with detection positions overlapping by  $4/11$  of the PSF diameter and by  $4/5$  of the transient duration. As the *XMM*-Newton PSF radius changes only modestly with off-axis angle, a changing PSF size will not affect our results.

A detection threshold significance is chosen so 0.01 false detections are expected per observation. Test volumes with a significant local elevation of counts are noted for later analysis.

### 3.3. Source Characterization

The list of candidate XRF events for each observation (typically containing  $\sim 300$  events) is then reduced. Each observation contains periods of high background, in which the count rate may be more than an order of magnitude higher than the average value during the observation. These periods often have a rise time comparable to the transient search length (see Figure 2), and give rise to spurious detections. We therefore remove sources that occur within high background periods. A high background period is found (and defined) as follows:

1. Split the detector into a  $10 \times 10$  grid of rectangular spatial regions.
2. Find the time-averaged countrate for the entire observation in each region.
3. For each region, rebin the event list into time periods of one nominal transient

duration (10 s). Any bin with a count rate  $> 3 \times$  the time-averaged count rate for that region is flagged as a possible high background bin for that region.

4. To avoid counting a very bright transient as a background flare, only time bins in which  $> 4$  regions are flagged as possible high background are flagged as whole-chip background flares.
5. Steps 2–4 are repeated three times, taking the time average only over periods not flagged as high background.

If necessary, the remaining sources are flagged as redundant - any particular transient is likely to be detected more than once due to the spatial and temporal overlaps in the detection algorithm. Candidate events close to the edge of chips (defined as sources with PSFs containing regions with fractional exposure  $< 0.35$ ) are removed.

Poisson variations in count rate within a few PSF distance of a bright X-ray source can also produce false detections. These bright sources are found manually by the presence of a great (1000+) excesses of false detections around a bright source. All candidate events in a circular area with a radius of 7 PSFs centered on the bright source are removed; in practice, this step is most efficiently performed by setting that portion of the detector exposure map to zero in the initial *celldetect* algorithm. A final manual inspection of the remaining sources removes sources near obvious detector anomalies, such as flickering pixels.

The candidate events which remain after this filtering we consider to be confirmed events.

### 3.4. Detection Sensitivity

To determine our detection sensitivity, we performed the following simulations.

Five-thousand test transients were initially added to each dataset separate from the detection runs. In each test transient photon-counts were distributed following Gaussian spatial and time profiles (90% diameter of 1 PSF and 90% duration of 10 s). The transients were randomly distributed in a 30' diameter circle centered on the telescope axis, carefully avoiding overlapping in the space-time volume.

The numbers of test transients detected by the *celldetect* algorithm at an incoming flux per transient of  $7.1 \times 10^{-13}$  erg cm $^{-2}$  s $^{-1}$  (10 total counts, on-axis) and separately at  $1.4 \times 10^{-11}$  erg cm $^{-2}$  s $^{-1}$  (200 total counts, on-axis) were recorded. An XRF photon spectral index of 2 was assumed and fluxes are measured over one detection time bin, 2.34 s.

Off-axis exposure and PSF radius variations were included, as were the effects of chip edges, hot pixels and other detector anomalies.

## 4. Results

### 4.1. Candidate Events

We found two candidate events – non-Poissonian excesses of counts over their local background – in the *XMM*-Newton-EPIC-pn observations. The characteristics of the detections are given in Table 3 and their distribution on the PN detector is given in Figure 1. Figure 2 illustrates that neither of our events were due to background flares.

To calculate the total number of counts detected over both events, we correct for the differing exposures of the source and background regions. This small (O[5% of counts]) effect is due to exposure variations across the telescope. Correcting for this effect, we find a total of  $15 \pm 3.8$  counts, including a background of  $0.37 \pm 0.16$  counts on the pn detector.

It should be noted that the candidate events occur within 2 PSFs of chip edges (Figure 1), and as such may be chip edge effects. Additionally, all counts comprising the event in observation 0125300101 are within one detector time bin (73 ms), which could also suggest a detector effect.

### 4.2. Non-Confirmation of the Astrophysical Nature of the Confirmed Events, with the MOS Detectors

The *XMM*-Newton-EPIC/MOS detectors observe the same area of sky fully simultaneously with the pn detector. Therefore, flux from a transient observed with the pn detector should also be detected by the MOS chips, albeit at a lower count rate.

Integrating over both of the confirmed events in the pn detector, a total of 0 counts were detected by the sum of both MOS detectors at the same sky locations (1 PSF spatial bin) and times (10s time bin), in a total estimated local background of  $0.55 \pm 0.16$  counts. Correcting for the fractional exposure difference between the MOS and PN detectors (but not their different detector efficiencies) gives a background of  $0.52 \pm 0.15$  counts.

We compare the detected MOS counts with those expected from the pn counts. The relative efficiency of the two MOS detectors, for a source of photon spectral slope of  $\alpha=1.2$  is 50%. Thus, we would expect  $7.5 \pm 1.9$  counts in the MOS detectors above background,

instead of the  $< 2$  counts (90% confidence) observed. We therefore place an upper-limit of  $< 27\%$  of the detected confirmed pn events being astrophysical in origin – i.e. neither of our events can be confirmed at the  $3\text{-}\sigma$  level.

### 4.3. Detection Sensitivity

The numbers of test transients detected at each flux level for each observation are given in Table 2. Observations with low detection sensitivities ( $< 100$  test transients detected) had sensitivity uncertainties reduced by repeating the Monte Carlo trials several times. Two observations (0114120101 and 0097820101) had very low ( $< 0.05\%$ ) detection sensitivities at the 10-count level; we do not include these observations in our calculations at that flux level.

### 4.4. Derived Limits on the Full-Sky XRF Event Rate

To obtain the upper-limits on the full sky XRF rate, we take our observed upper-limit to be  $< 1$  event at the two transient fluxes described above. To calculate our total exposure, we use the detector area (a circle of radius  $15'$ ), the total ontime and the detection fraction from Table 4. Since our detection fractions assumed the spatial distribution to be homogenous across the detector, these fractions take into account the presence of bright sources, low-exposure pixels, edge effects and lost detector columns. The fractions also include sensitivity losses due to ontime during which background flares occurred. The total exposure is therefore  $0.19 \text{ sq deg} \times \sum_i (T_{\text{ontime}} \times D_{\text{fraction}})$ , where  $i$  is for each of six observations,  $T_{\text{ontime}}$  is the time per observation, and  $D_{\text{fraction}}$  is the event detection fraction, which is a function of the number of counts per event.

At the flux limit corresponding to 10 counts the total exposure is  $0.19 \text{ sq deg} \times 1700 \text{ s}$ ; at 200 counts, the total exposure is  $0.19 \text{ sq deg} \times 101000 \text{ s}$ . The correction factors to  $\text{events sky}^{-1} \text{ yr}^{-1}$  are  $5.5 \times 10^8$  and  $8.0 \times 10^6$  respectively. The corresponding XRF event rate limits are therefore  $< 6.2 \times 10^9 \text{ events sky}^{-1} \text{ yr}^{-1}$  at 10 counts per transient and  $< 1.0 \times 10^8 \text{ events sky}^{-1} \text{ yr}^{-1}$  at 200 counts per transient. This number of counts per time-bin corresponds to average fluxes of  $7.1 \times 10^{-13} \text{ erg cm}^{-2} \text{ s}^{-1}$  and  $1.0 \times 10^8 \text{ events sky}^{-1} \text{ yr}^{-1}$  for  $1.4 \times 10^{-11} \text{ erg cm}^{-2} \text{ s}^{-1}$  respectively, assuming a spectral power-law photon index  $\alpha=2$ .

Figure 3 shows the relation of our upper limits to a previous result (Vikhlinin 1998), as well as to an extrapolation from the *BeppoSAX*/WFC XRF rate assuming a homogenous source population. Our limit is less stringent than the previous result by a factor of



$\sim 2000$ , due in large part to the factor  $\sim 13$  greater size FOV of the ROSAT/PSPC detector over the pn detector and the longer integration time of the previous result. The limits are also consistent with the extrapolation of the *BeppoSAX*/WFC XRF rate assuming a homogenous source population.

We find a 90% upper limit on the number of flashes per sky per year for two fluxes:  $6.2 \times 10^9 \text{ events sky}^{-1} \text{ yr}^{-1}$  for a flux of  $7.1 \times 10^{-13} \text{ erg cm}^{-2} \text{ s}^{-1}$  and  $< 1.0 \times 10^8 \text{ events sky}^{-1} \text{ yr}^{-1}$  for  $1.4 \times 10^{-11} \text{ erg cm}^{-2} \text{ s}^{-1}$  both assuming a spectral power-law photon index  $\alpha=2$ .

## 5. Discussion and Conclusions

We conduct searches for flashes in the XMM-Newton public archival data, specifically those observations with total observation time  $> 50 \text{ ks}$  and with galactic latitude  $< -15 \text{ deg}$  or  $> 15 \text{ deg}$ . We use a *celldetect* algorithm extended to include three dimensions (two spatial, one temporal). Detected sources are categorized, and non-astronomical sources flagged. Two candidate events were found in EPIC/pn data, with a total of  $15 \pm 3.8$  counts in a total estimated background of  $0.37 \pm 0.16$  counts. The astrophysical nature of these candidate events is not confirmed by fully simultaneous observations with the EPIC/MOS detectors, and we conclude that we have detected no astrophysical XRFs. We suggest that the events as observed may be due to detector effects.

From this we place full-sky, 90% confidence upper-limits on the XRF event rate of  $< 6.2 \times 10^9 \text{ events sky}^{-1} \text{ yr}^{-1}$  (at  $7.1 \times 10^{-13} \text{ erg cm}^{-2} \text{ s}^{-1}$ ) and  $< 1.0 \times 10^8 \text{ events sky}^{-1} \text{ yr}^{-1}$  (at  $1.4 \times 10^{-11} \text{ erg cm}^{-2} \text{ s}^{-1}$ ). The high-flux limit is above a previous limit obtained with *ROSAT*, by a factor of  $\sim 2000$ , due to the larger FOV and integration time of the PSPC data. The limit at the lower flux remains above that extrapolated from the *BeppoSAX*/WFC events assuming homogeneity.

The *ROSAT* limit remains the most stringent limit on an extrapolation of the XRF burst rate to lower-fluxes, and implies that the assumption of homogeneity is violated at a flux  $> 2 \times 10^{-11} \text{ erg cm}^{-2} \text{ s}^{-1}$ . To obtain a limit similar in magnitude to the *ROSAT* limit, using XMM/pn, a total integration time of  $\sim 2 \times 10^8$  seconds is required, which will likely not be obtained with this instrument due to finite instrument lifetime. It is unclear whether the XRFs observed with *BeppoSAX*/WFC are consistent or inconsistent with homogeneity; and so it may be that a break in the number-fluence distribution, as observed in GRBs, takes place at a flux at or above that probed by the *BeppoSAX*/WFC observations.

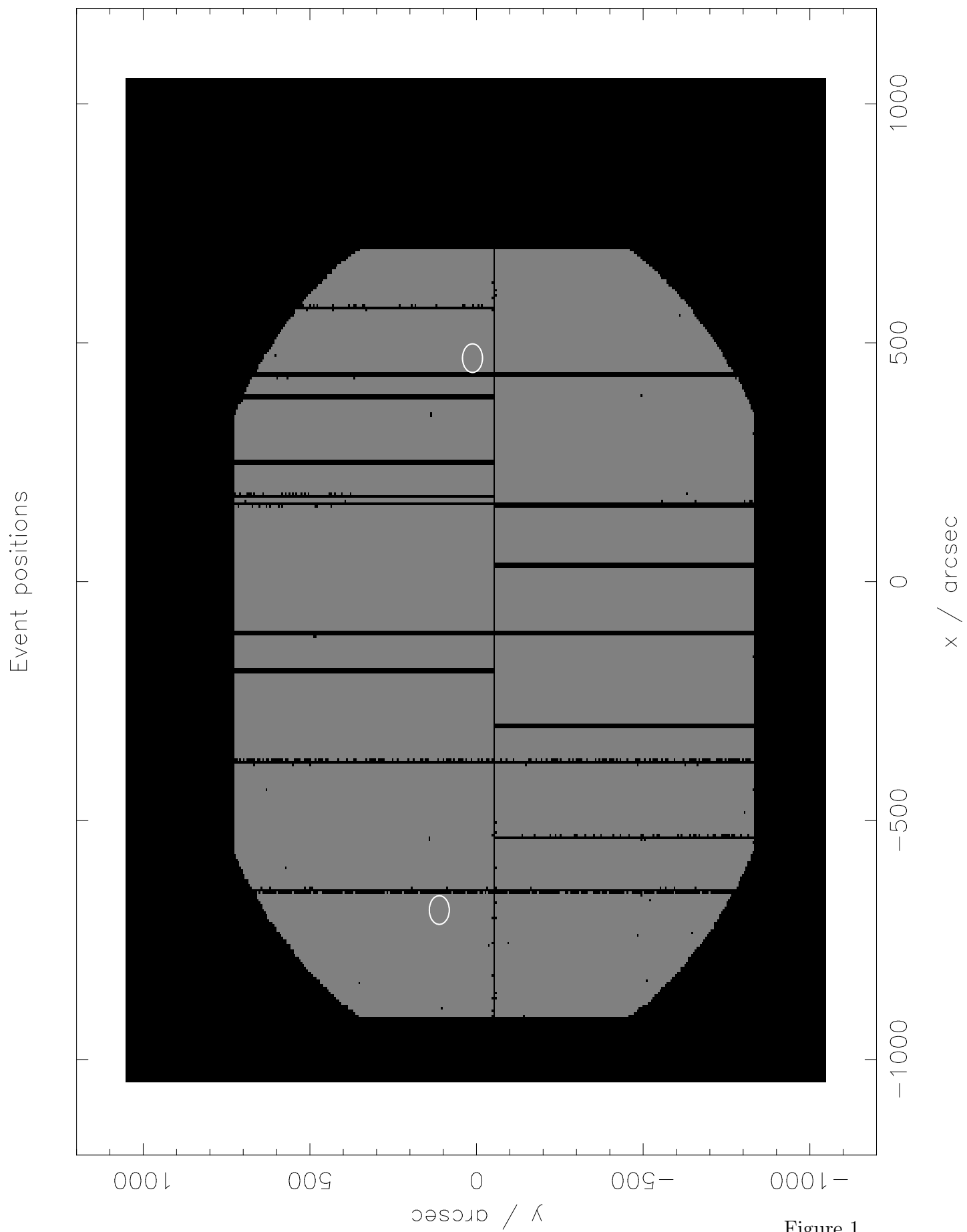
## References

- Fruchter, A., Pattel, S., Kouveliotou, C., Rhoads, J., Holland, S., Burud, I., & Wijers, R., 2002a, *GRB Circular Network* 1268
- Fruchter, A., Rhoads, J., Burud, I., Levan, A., Patel, S., Kouveliotou, C., Gorosabel, J., & Hjorth, J., 2002b, *GRB Circular Network* 1440
- Gotthelf, E. V., Hamilton, T. T., & Helfand, D. J., 1996, *ApJ* 466, 779
- Heise, J. & in 't Zand, J., 2001, *Proceedings of the Jan van Paradijs Memorial Symposium 'From X-ray Binaries to Gamma Ray Bursts', Amsterdam June 6-8 2001*, astro-ph/0112353
- Heise, J., in 't Zand, J. M. M., & Kulkarni, S., 2002, *Nature*, submitted
- Lewin, W., Van Paradijs, J., & Taam, R., 1993, *Space Sci. Rev.* 62, 223
- Paciesas, W., Meegan, C., Pendleton, G., Briggs, M., Kouveliotou, C., Koshut, T., Lestrade, J., McCollough, M., Brainerd, J., Hakkila, J., Henze, W., Preece, R., Connaughton, V., Kippen, R., Mallozzi, R., Fishman, G., Richardson, G., & Sahi, M., 1999, *The Astrophysical Journal Supplement Series, Volume 122, Issue 2, pp. 465-495*
- Vikhlinin, A., 1998, *ApJ* 505, L123

Fig. 1.— Detected transient positions on the detector chip. The chip layout shown is from the raw count positions of observation 097820101.

Fig. 2.— Detected transient times. Total detector light curves are shown, binned into the detection time bins of 2.34 seconds. Detected transient times are shown by arrows. The large positive excursions are due to total-detector increases in the background countrate. Observation 0114120101 has a generally elevated count rate because of a very bright source in the center of the frame. The periods with reduced count numbers in 0114120101 are due to CCD dead time.

Fig. 3.— Cumulative histogram of numbers of detected GRBs and XRFs as a function of fluence. We show our upper limits with bars and arrows. The BATSE triggered GRBs are normalised to 666 flashes/year/full sky at BATSE's minimum detection fluence (Paciesas et al. 1999). The BeppoSAX and BATSE XRFs normalisation is approximated by the same factor, after taking the different exposure times of the datasets onto account. An extrapolation of a  $-3/2$  power-law is shown from the XRFs detected with BeppoSAX and BATSE. XMM (a) is our 90% upper limit at 10 counts per XRF, XMM (b) is our 90% upper limit at 200 counts per XRF. Both limits are derived with an energy pass-band of 1.4-15 keV. The figure also shows the 90% ROSAT upper limit with an energy pass-band of 0.5-2 keV (Vikhlinin 1998).



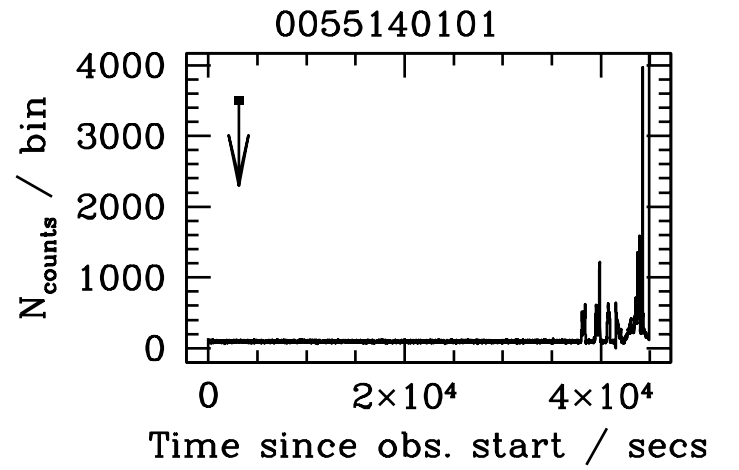
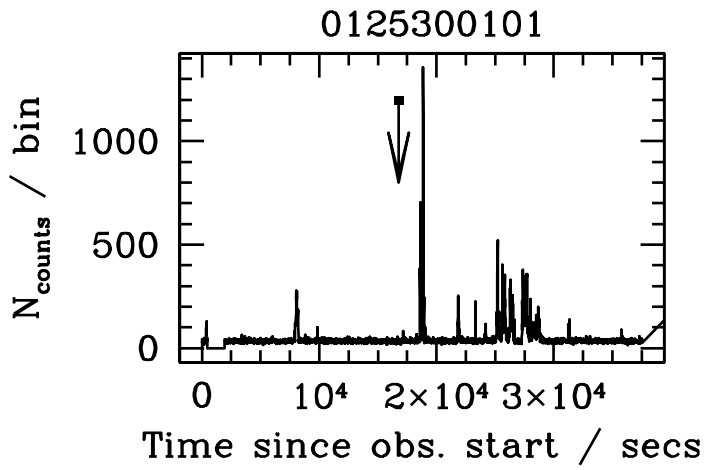
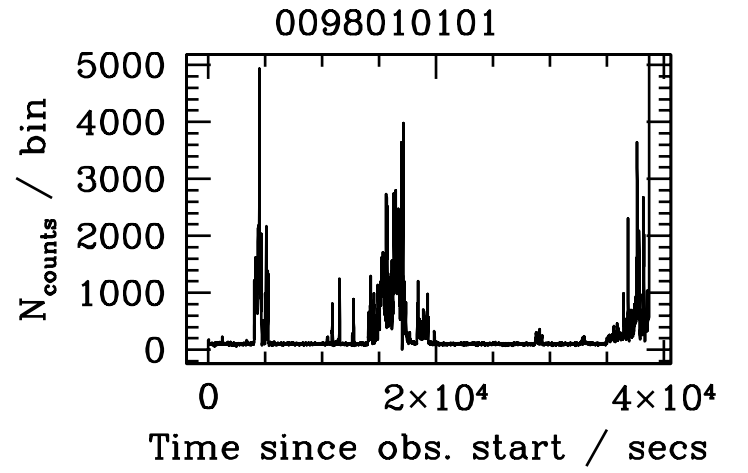
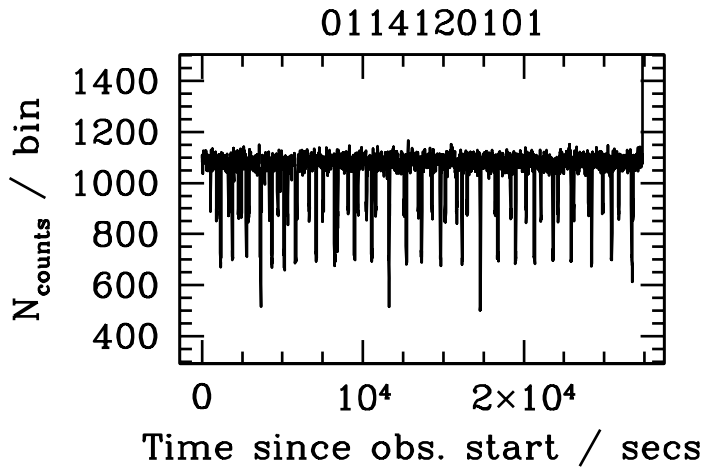
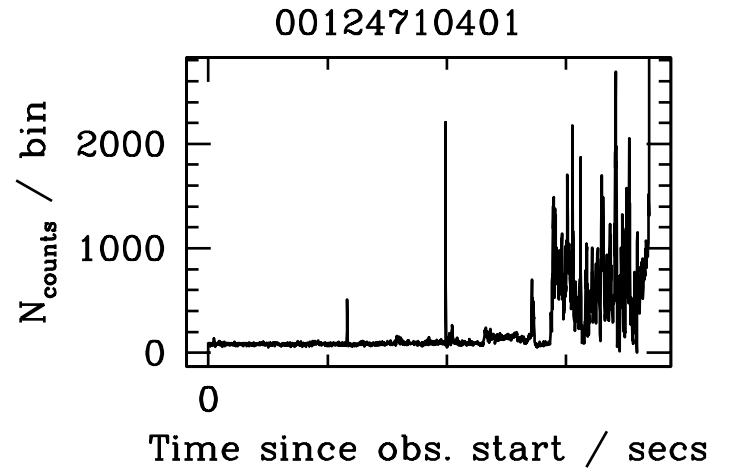
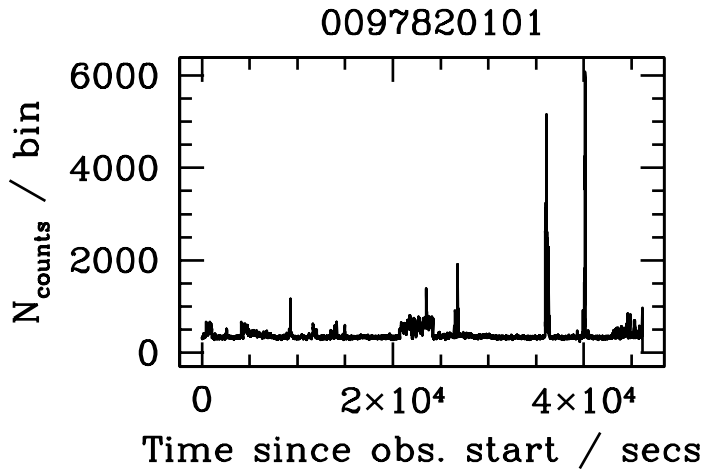


Figure 2

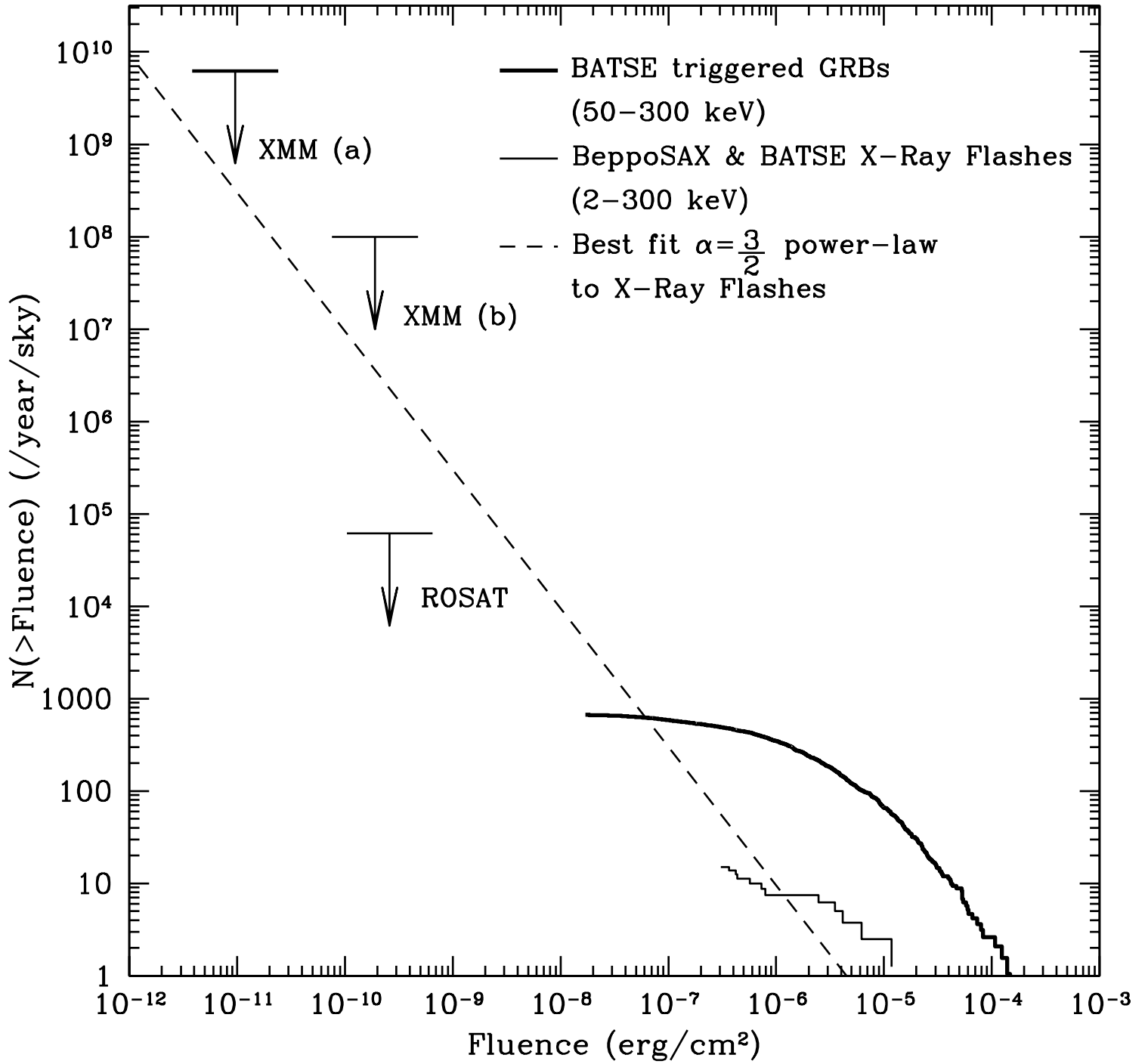


Figure 3

## Appendix

We give detailed information on each of the detections in Figures 4 to 5. In each figure, we show: (top left) the low time resolution (2.34 sec/bin) light curve within 1 PSF of the candidate event position (the central bin, plus the adjacent bins; (top middle) the high time resolution (0.076 sec) lightcurve; (top right) the lightcurve of the pn detector (bottom left) the position in the pn detector where the event was found; (bottom middle) the location of the individual counts events within the detect cell; and (bottom right) the binned energy values for the individual count events within the detect cell.

Detector	Chandra ACIS		XMM EPIC PN		XMM EPIC MOS	
Flash photon index	$\alpha = 1.2$	$\alpha = 2.0$	$\alpha = 1.2$	$\alpha = 2.0$	$\alpha = 1.2$	$\alpha = 2.0$
Events/year/sky	$6.3 \times 10^7$	$1.5 \times 10^7$	$1.8 \times 10^7$	$4.8 \times 10^8$	$2.2 \times 10^6$	$3.0 \times 10^7$
Expected events	0.077	1.8	0.30	8.2	0.037	0.52

Table 1: Extrapolated event numbers based on flash detection numbers from WFC BeppoSAX, assuming a minimum of 1 count per second required for detection. Flash spectra are calculated using a power law model,  $I(E) \propto E^{-\alpha}$ ; the dataset was chosen as described in section 3.1. The expected event numbers are given for all datasets taken together. The  $\alpha = 1.2$  model may imply a spectral cut-off in XRFs, so avoiding fluence in the high energy band.

Observation #	Total ontime (s)	Total good time (s)	Detections at 10 counts	Detections at 200 counts	# trials
0055140101	45257.2	41266.6	0.51±0.05%	61.8±1.1%	8,332,408
0097820101 *	47721.2	37620.9	0.040±0.009%	38.4±0.9%	7,231,281
0098010101 *	42121.1	27760.7	0.22±0.03%	32.2±0.8%	5,144,553
0114120101 *	30453.4	30453.4	0.0%	46.8±1.0%	5,982,074
0124710401	19939.2	12505.8	0.98±0.14%	41.1±0.9%	1,211,285
0125300101	39599.4	28526.8	2.9±0.2%	47.8±0.98%	4,983,749

Table 2: Test transient detection efficiency. Good time is the total time of sections of the observation outside background flares, as defined in section 3.3. Transients are only detected in the good time - note that test transients are placed throughout the ontime. 10 counts corresponds to an on-axis flux of  $7.1 \times 10^{-13}$  erg cm $^{-2}$  s $^{-1}$  200 counts to  $1.4 \times 10^{-11}$  erg cm $^{-2}$  s $^{-1}$ . Test photon-counts are placed in a Gaussian distribution, with 90% within 5 seconds and 1 PSF of the test transient location. The number of trials given is the number of individual tests for significance made on the observation; the significance of a particular foreground count excess is multiplied by the number of trials to obtain its probability. The same number of trials is made in both the test transient detection and the observed transient detection and depends on both observation duration and the details of the observation's exposure map. The number has been corrected to include only trials in the good time. Observations marked with \* have central bright sources removed. 0097820101 has an additional off-axis bright source removed.

Observation #	Target	Event #	Expected counts PN/MOS	Detected counts PN/MOS	$\langle E_{count} \rangle$ / keV	$F_{peak}$ / ergs/cm $^2$ / sec	Fluence / ergs/cm $^2$	$\langle RA \rangle$	$\langle DEC \rangle$	$\sigma(pos^n)$ (statistical uncertainty) / "	$T_0$ / sec
0055140101	LP 944-20	1	0.15 ± 0.11 / 0.20 ± 0.10	7.0 ± 2.6 / 0	4.73	$8.11 \times 10^{-13}$	$6.65 \times 10^{-12}$	03:40:17.5	- 35:20:15.8	16.8	95271781
0097820101	A 1795	-	-	-	-	-	-	-	-	-	-
0098010101	A 1835	-	-	-	-	-	-	-	-	-	-
0114120101	M87	-	-	-	-	-	-	-	-	-	-
0124710401	Coma 4	-	-	-	-	-	-	-	-	-	-
0125300101	J104433.04-012502.2	1	0.22 ± 0.11 / 0.35 ± 0.12	8.0 ± 2.8 / 0	6.92	$3.2 \times 10^{-12}$	$7.6 \times 10^{-12}$	10:44:4.0	-1:22:20.1	12.3	75915279

Table 3: Detected events. MOS counts have been corrected for the fractional exposure difference between the PN and MOS detectors, but not for the detectors' relative efficiencies. Peak flux is calculated over one detection time bin (2.34 s). Flux and fluence assume a photon index  $\alpha = 2$  and a passband of 0.4-15keV. The spectral index is the dominant uncertainty in the flux and fluence, with energy conversion factors ranging from  $4.3 \times 10^{-12}$  erg cm $^{-2}$  s $^{-1}$  count $^{-1}$  for  $\alpha = 1.2$  to  $1.2 \times 10^{-13}$  erg cm $^{-2}$  s $^{-1}$  count $^{-1}$  for  $\alpha = 3$ . Right ascension and declination are J2000.0, FK5.



Spectrum $\alpha$	$R \equiv \frac{c(\text{MOS1\&2})}{c(\text{PN})}$	PN counts / BG	MOS counts / BG	MOS: predicted counts	90% upper limit of astrophysical events	10 count event rate / sky / year	200 count event rate / sky / year
-1	0.48	$15.0 \pm 3.8$ / $0.37 \pm 0.16$	$0.0 \pm 0.0$ / $0.52 \pm 0.15$	$7.5 \pm 1.8$	25%	$6.2 \times 10^9$	$1.0 \times 10^8$
0	0.57	...	...	$8.8 \pm 2.2$	21%	$6.2 \times 10^9$	$1.0 \times 10^8$
1	0.54	...	...	$8.4 \pm 2.1$	22%	$6.2 \times 10^9$	$1.0 \times 10^8$
2	0.32	...	...	$5.2 \pm 1.2$	37%	$6.2 \times 10^9$	$1.0 \times 10^8$
3	0.19	...	...	$3.3 \pm 0.7$	63%	$6.2 \times 10^9$	$1.0 \times 10^8$

Table 4: The expected 90% upper flash rate limit for a number of assumed flash photon indices. The two event fluences are those given in the detection sensitivity calculations. The PN to MOS ratio (R) assumes a passband of 0.4-15keV. As our spectral assumptions indicate neither of the detected events are astrophysical we set the upper limit event number to be 1.

Fig. 4.— 0055140101 Event 1.

Fig. 5.— 0125300101 Event 1.

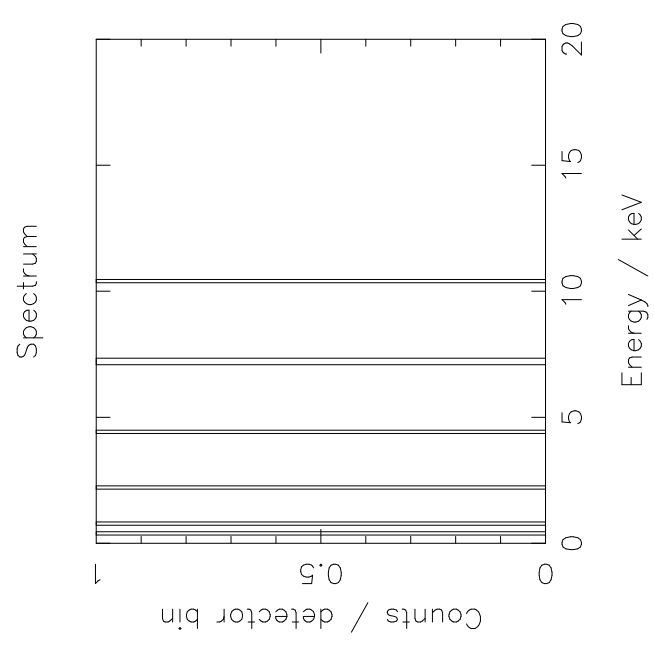
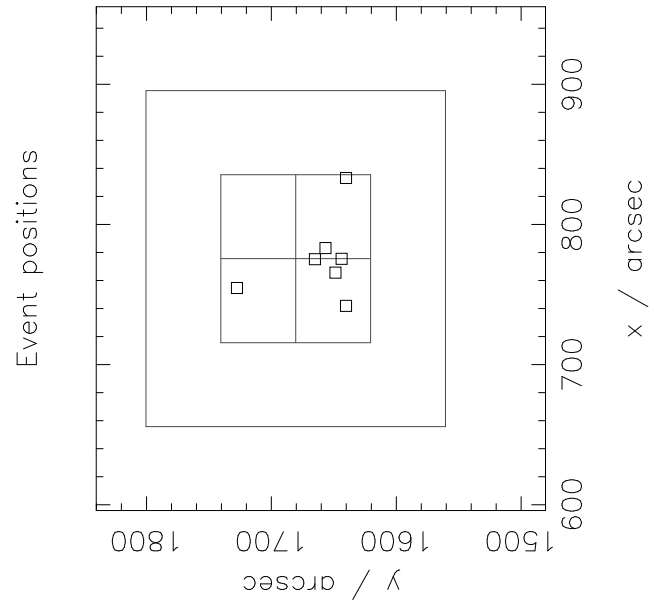
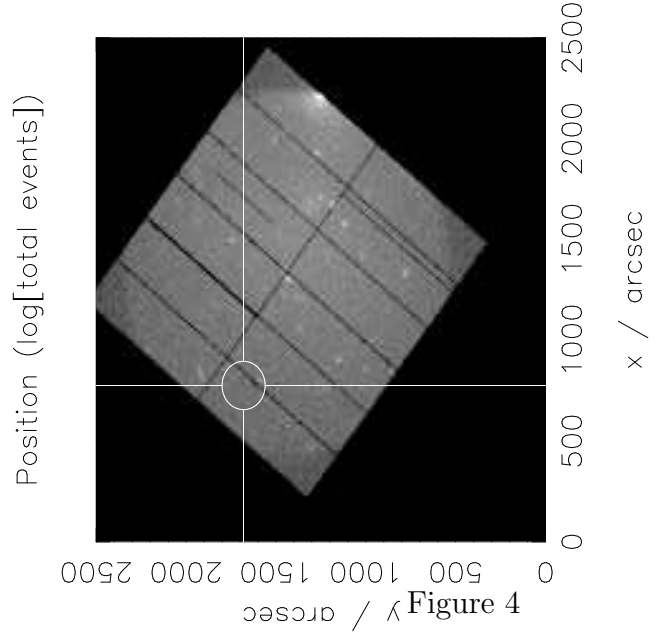
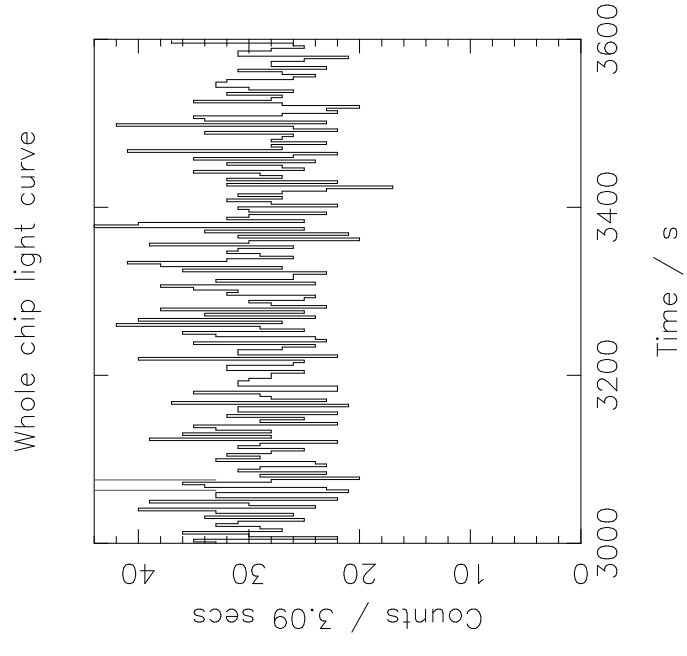
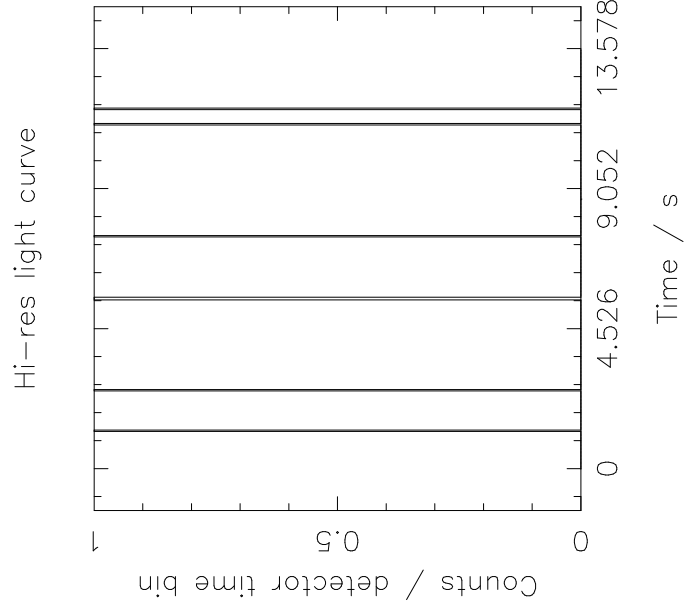
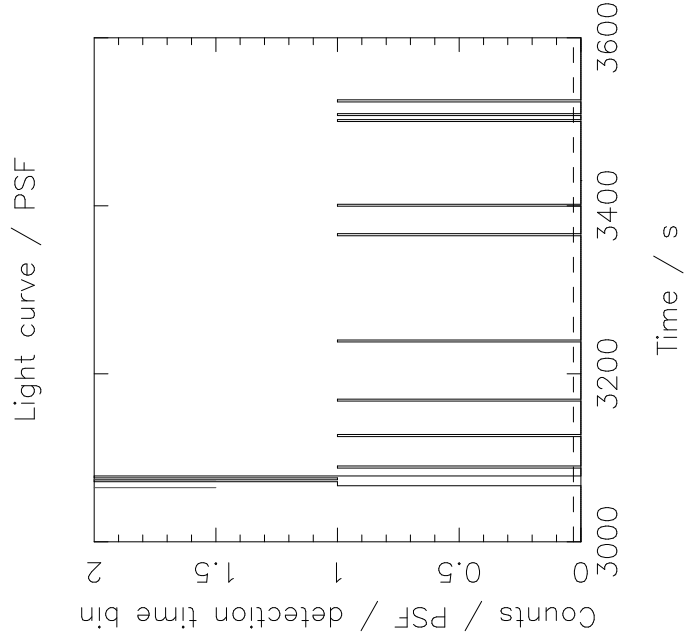
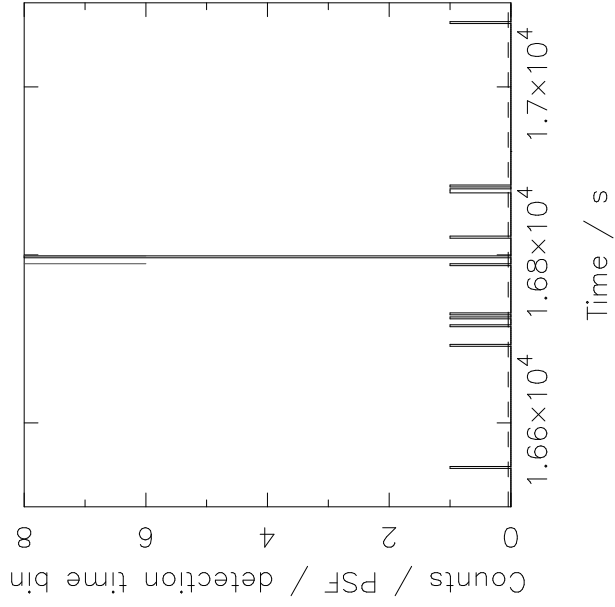
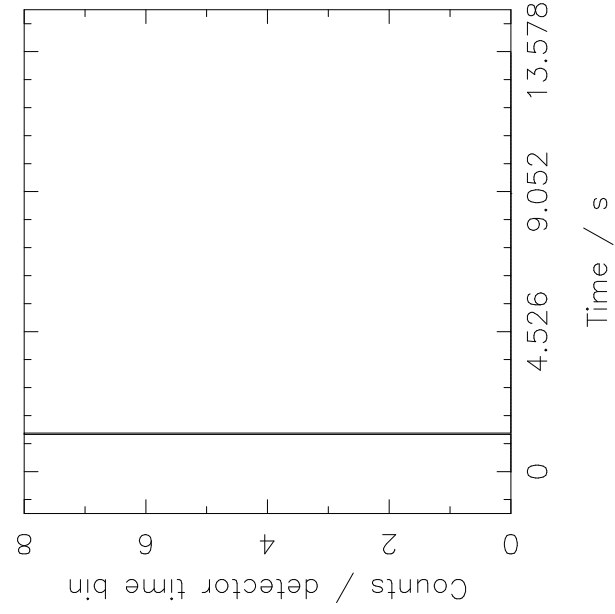


Figure 4

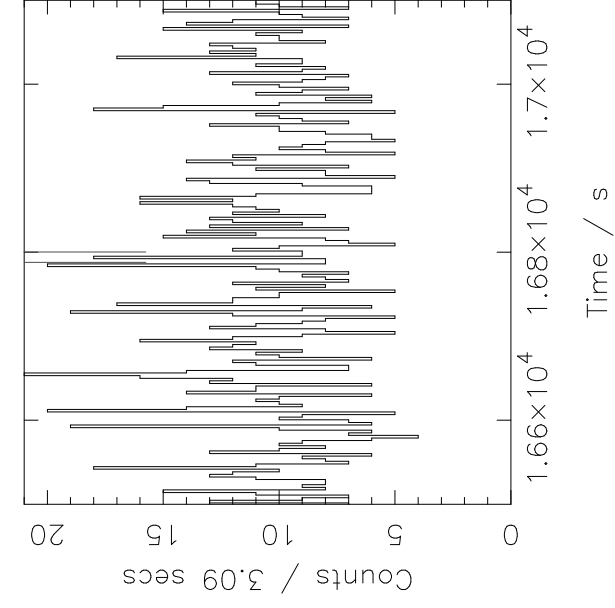
Light curve / PSF



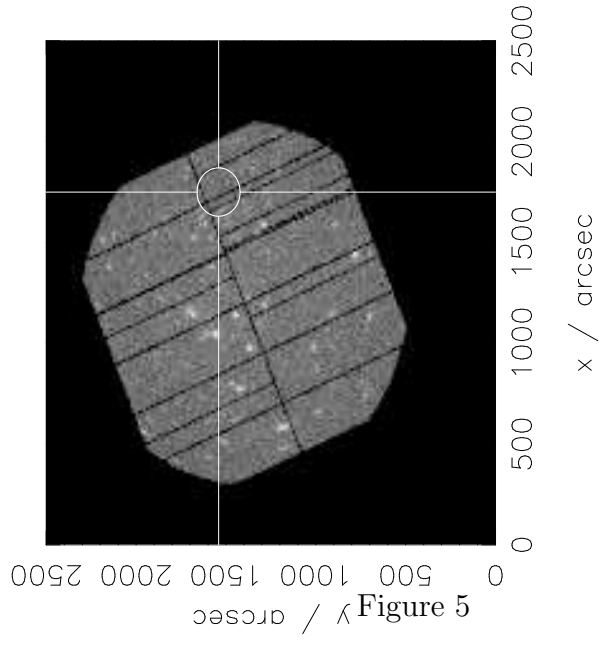
Hi-res light curve



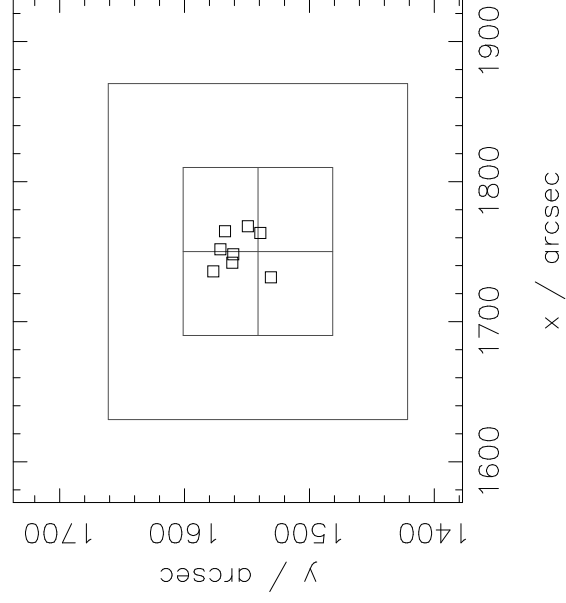
Whole chip light curve



Position (log[total events])



Event positions



Spectrum

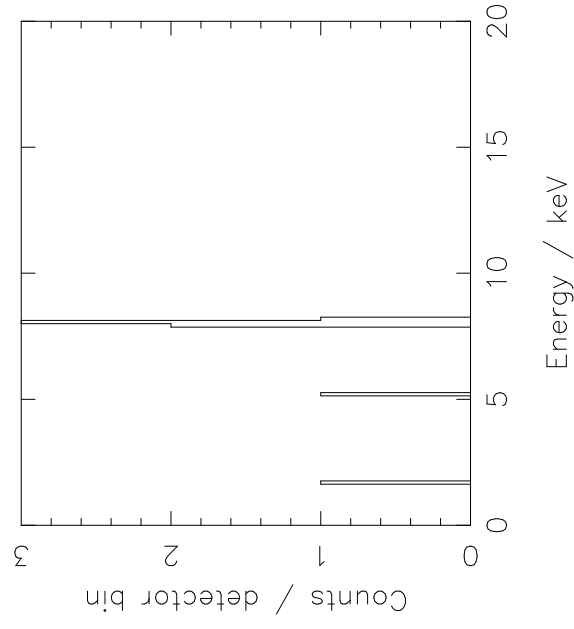


Figure 5